

# The Chemical link between stars and their rocky planets

Vardan Adibekyan,<sup>1,2\*</sup> Caroline Dorn,<sup>3</sup> Sérgio G. Sousa,<sup>2</sup>  
Nuno C. Santos,<sup>1,2</sup> Bertram Bitsch,<sup>4</sup> Garik Israelian,<sup>5,6</sup> Christoph Mordasini,<sup>7</sup>  
Susana C. C. Barros,<sup>1,2</sup> Elisa Delgado Mena,<sup>1</sup> Olivier D. S. Demangeon,<sup>1,2</sup>  
João P. Faria,<sup>1</sup> Pedro Figueira,<sup>9,1</sup> Artur A. Hakobyan,<sup>8</sup>  
Mahmoudreza Oshagh,<sup>5,6</sup> Masanobu Kunitomo,<sup>10</sup> Yoichi Takeda,<sup>11,12</sup>  
Emiliano Jofré,<sup>13,14,15</sup> Romina Petrucci,<sup>14,15</sup> Eder Martioli,<sup>16,17</sup>

<sup>1</sup>Instituto de Astrofísica e Ciências do Espaço, Universidade do Porto, CAUP, Rua das Estrelas, 4150-762 Porto, Portugal

<sup>2</sup>Departamento de Física e Astronomia, Faculdade de Ciências,

Universidade do Porto, Rua do Campo Alegre, 4169-007 Porto, Portugal

<sup>3</sup>University of Zurich, Institut of Computational Sciences, Winterthurerstrasse 190, CH-8057, Zurich, Switzerland

<sup>4</sup>Max-Planck-Institut für Astronomie, Königstuhl 17, 69117, Heidelberg, Germany

<sup>5</sup>Instituto de Astrofísica de Canarias, E-38205 La Laguna, Tenerife, Spain

<sup>6</sup>Departamento de Astrofísica, Universidad de La Laguna, E-38206 La Laguna, Tenerife, Spain

<sup>7</sup>Physikalisches Institut, University of Bern, Gesellschaftsstrasse 6, 3012, Bern, Switzerland

<sup>8</sup>Center for Cosmology and Astrophysics, Alikhanian National Science Laboratory, 2

Alikhanian Brothers Str., 0036 Yerevan, Armenia

<sup>9</sup>European Southern Observatory, Alonso de Córdova 3107, Vitacura, Región Metropolitana, Chile

<sup>10</sup>Department of Physics, School of Medicine, Kurume University, 67 Asahimachi, Kurume, Fukuoka 830-0011, Japan

<sup>11</sup>National Astronomical Observatory, 2-21-1 Osawa, Mitaka, Tokyo 181-8588, Japan

<sup>12</sup>SOKENDAI, The Graduate University for Advanced Studies, 2-21-1 Osawa, Mitaka, Tokyo 181-8588, Japan

<sup>13</sup>Instituto de Astronomía, Universidad Nacional Autónoma de México, Ciudad Universitaria, CDMX, C.P. 04510, México

<sup>14</sup>Universidad Nacional de Córdoba (OAC), Laprida 854, X5000BGR, Córdoba, Argentina

<sup>15</sup>Consejo Nacional de Investigaciones Científicas y Técnicas (CONICET), Argentina

<sup>16</sup>Institut d'Astrophysique de Paris, UMR7095 CNRS,

Université Pierre & Marie Curie, 98 bis Boulevard Arago, 75014 Paris, France

<sup>17</sup>Laboratório Nacional de Astrofísica, Rua Estados Unidos 154, Itajubá/MG 37504-364, Brazil

\*E-mail: vadibekyan@astro.up.pt

**Young stars and planets both grow by accreting material from the proto-stellar disks. Planetary structure and formation models assume a common origin of the building blocks, yet, thus far, there is no direct conclusive observational evidence correlating the composition of rocky planets to their host stars. Here we present evidence of a chemical link between rocky planets and their host stars. The iron-mass fraction of the most precisely characterized rocky planets is compared to that of their building blocks, as inferred from the atmospheric composition of their host stars. We find a clear and statistically significant correlation between the two. We also find that this correlation is not one-to-one, owing to the disk-chemistry and planet formation processes. Therefore rocky planet composition depends on the chemical composition of the proto-planetary disk and contains signatures about planet formation processes.**

Low-mass transiting planets orbiting bright, nearby stars with radial-velocity (RV) follow-up observations are ideal targets for interior characterization studies. These are enabled by the combination of RV and transit techniques, that determine the two fundamental parameters: planetary radius via transit observations and planetary mass via RV measurements. The derivation of these parameters, however, relies on the knowledge of the properties of the host stars. In this respect, planets orbiting solar-type stars (FGK spectral types) are of primary interest because of our ability to characterize them most accurately, and their accuracy depends on the accuracy of the same parameter as measured for the star (1, 2).

Thanks to very high-precision spectroscopic and photometric (transit) measurements, 32 well-characterized (with an uncertainty both in mass and radius below 30%) low-mass exoplanets ( $M < 10 M_{\oplus}$ ) orbiting 27 solar-type stars are currently known (see Materials and Methods). The distribution of these planets on the mass-radius diagram is shown in Fig.1. A clear gap in radius can be seen (see top panel of Fig. 2) for planets with masses greater than about  $4 M_{\oplus}$ . This gap is suggested to separate

rocky planets from the water- and gas-rich mini-Neptunes (3–7).

In this work we explore the link between the properties of rocky planets and the chemical composition of their host stars. For this reason, here we focus only on 22 planets located on the bottom part of the Radius Valley i.e. planets without significant water or gas-rich envelopes.

It is generally believed that the atmospheric elemental abundances (except the lightest elements) of sun-like stars are preserved during the stellar main sequence phase within a few percent (8). For most of the nonvolatile elements the solar photospheric and meteoritic abundances were shown to be in good agreement (8). In addition, it has been shown that the Fe/Si and Mg/Si abundance ratios in stars and planetary bulk remain very similar during the planet formation processes (9–11). As such, the atmospheric abundances of refractory elements (e.g. Mg, Si, and Fe) of solar-type stars are usually considered as a proxy of the composition of the initial proto-planetary disk and their building blocks (12, 13). We have collected spectra from different instruments for the host stars of the planets selected with the aim of determining their atmospheric chemical composition (see Materials and Methods). In particular we determined the abundances of C, O, Mg, Si, and Fe, which together with H are the most relevant elements controlling the species expected from equilibrium condensation models (14). On a second step, we have inserted these abundances in a simple stoichiometric model (15, 16) to estimate the iron-to-silicate mass fraction ( $f_{\text{iron,star}}$ ) of planetary building blocks. For the solar system planet building blocks, this model predicts a  $f_{\text{iron,star}}$  of  $33.2 \pm 1.7\%$ , a value very similar to the iron content of the Earth ( $\sim 32\%$ ) (17).

As can be seen from the top panel of Fig. 2, for a given mass the rocky planets of our sample show some dispersion in radius around the Earth-like composition curve. To understand whether the densities of the planets are linked to the primordial composition of the planet building blocks, in the bottom panel of Fig. 2 we show the normalized planet density,  $\rho/\rho_{\text{Earth-like}}$ , as a function of  $f_{\text{iron,star}}$ . The normalization parameter  $\rho_{\text{Earth-like}}$ , is the density of a planet with Earth-like composition (18) for a given mass. The normalization is important because planets with the same composition have different densities depending on their mass due to compression. The figure reveals a clear correlation

(see Materials and Methods for details about the performed statistical tests and their results) between these two quantities indicating that the final planetary density is a function of the composition of the planet building blocks.

Since one of these quantities is linked exclusively to the observed properties of the planets while the other one is linked to the host star composition, this trend provides the first observational evidence for the chemical link between stars and their rocky planets. This result suggests that rocky planets preserve information about the overall chemical composition of the proto-planetary disk in which they are formed.

Despite the general trend observed on the bottom panel of Fig. 2, it is evident that for a given  $f_{\text{iron,star}}$  (i.e. stellar and pebble/planetesimal composition) rocky planets can have a range of densities. Although the observed scatter is compatible with the average uncertainty of  $\rho/\rho_{\text{Earth-like}}$ , we tested whether part of this dispersion can have an astrophysical origin. One of the parameters that might influence the size and thus density of planets is the flux (high-energy photons) that planets receive from their host stars (6, 19). We found, however, no correlation between the normalized density of the planets and their equilibrium temperature,  $T_{\text{eq}}$  (see the absence of a color gradient in the bottom panel of Fig. 2), suggesting that for rocky planets  $T_{\text{eq}}$  does not have a major impact on their radius (20).

The next logical step was to study how different the final iron mass fraction of the planets can be when compared with the iron-mass fraction of the primordial planet-building blocks as estimated from the host star composition. Based on planet interior models (18), we determined the possible iron mass fraction of the planets ( $f_{\text{iron,planet}}$ ) using only their mass and radius. We considered two scenarios i) assuming iron is present only in the core and ii) assuming iron is present both in the core and mantle of the planets. In Fig. 3 we show the dependence of  $f_{\text{iron,planet}}$  on  $f_{\text{iron,star}}$ . Two interesting conclusions can be drawn from this figure. First, the iron mass fraction of planets is a function of the iron-mass fraction of the primordial planet building-blocks, i.e., the two quantities show a statistically significant correlation for a monotonic dependence. Second, the planets span wider range of iron-mass fraction than their primordial building-blocks. It is interesting to note that the overall

distribution of core-mass fraction (which can be related to the iron mass fraction) of rocky planets was shown to be wider than the overall distribution of exoplanet host stars (20).

It was recently suggested that the iron fraction in planets can be significantly increased due to the recondensation of evaporated pebbles (21). In this model, planets formed close to rocklines (regions where refractory material condensates/sublimates) can have an increased proportion of iron when compared with the proto-stellar value. This effect may explain the overall larger values of  $f_{\text{iron,planet}}$  when compared with the  $f_{\text{iron,star}}$ . Interestingly, the trend observed in Fig. 3 suggests that the aforementioned effect should depend on the stellar iron-mass fraction, meaning that stars with naturally higher iron fraction will see a larger increase of this effect (21).

In Fig. 3 one can potentially identify a group of five planets with relatively high content of iron when compared to the rest of the planets - the super-Earths. Several mechanisms of planet formation and evolution are proposed in the literature to explain the high-density and high  $f_{\text{iron,planet}}$  of these planets (22), sometimes called super-Mercuries. Although the number of these planets is not large preventing to make firm conclusion, one can still notice that they are orbiting stars with high  $f_{\text{iron,star}}$  i.e. stars with overabundance of Fe relative to Mg and Si. This may suggest that whatever is the mechanism responsible for the overabundance of iron in these planets, it should be related to the composition of the proto-planetary disk.

Appreciating the possibility that the super-Mercuries may had a specific origin and/or evolutionary path, we checked whether our findings hold for the rest of the planets. We found that the  $f_{\text{iron,planet}} - f_{\text{iron,star}}$  correlation remains significant for the sample of super-Earths. In addition, we found that the Fe/(Mg+Si) abundance ratio estimated for these planets shows a strong dependence on Fe/(Mg+Si) ratio of their host stars. The data reveals a non 1-to-1 relationship (see Materials and Methods) that, perhaps, should replace previously used 1-to-1 relationship.

Several attempts have been made in the past trying to link the composition of low-mass planets and their host stars. However, these attempts were either based on single planetary systems (23, 24), on a small sample of planets (15, 20, 22), or on a comparison of the overall properties of planets and overall

properties of planet host stars in a population sense (20). As a result, it was not possible to reach a firm and general conclusion either because of low-number statistics, because of the adopted non-optimal approach, or because the results were not as informative (especially if the composition of the stars are not derived in a homogeneous way) as they would be if a direct star-planet comparison was performed (see Materials and Methods). Our results clearly demonstrate the importance of performing a detailed chemical analysis of exoplanet hosts and making a direct star-planet comparison.

The observational results obtained in this work are important for two different reasons. First, as noted earlier, the information on the stellar relative abundance of major rock-forming elements such as Fe, Mg, Si is commonly used to improve interior estimates for rocky planets (12, 13) and has even been used to estimate planet composition in different galactic populations (16, 25, 26). In this context, the chemical link we observed validates the assumptions made in the aforementioned works. Second, the fact that the observed correlation between the  $f_{\text{iron,planet}}$  and  $f_{\text{iron,star}}$  is not one-to-one ( $f_{\text{iron,planet}}$  is larger than  $f_{\text{iron,star}}$ ) suggests that the proto-planetary disk chemistry (depending on the location of planets at the time of their formation) and specific processes acting during the formation of these planets play an important role for planetary composition. Moreover, our brief and only qualitative discussion on the possible origin of the overabundance of iron in planets when comparing to their primordial building blocks shows the potential of using these correlations for studying the specifics of rocky planet formation.

The detection and detailed characterization of rocky planets orbiting Sun-like stars is currently one of the main drivers for the development of large space-borne missions and ground-based instruments by the major international agencies (ESO, ESA, NASA). The number of well characterized rocky planets will continually increase in the near future thanks to projects such as TESS (NASA, 2018) (27), ESPRESSO (ESO, 2018) (28), CHEOPS (ESA, 2019) (29), and PLATO (ESA, 2026) (30). Performing an analysis similar to ours, but with significantly larger number and better characterized low-mass planets will without doubt help in constraining further the chemical link between stars and their rocky planets established in this manuscript.

## References

1. S. G. Sousa, N. C. Santos, M. Mayor, S. Udry, L. Casagrande, G. Israelian, F. Pepe, D. Queloz, M. J. P. F. G. Monteiro, Spectroscopic parameters for 451 stars in the HARPS GTO planet search program. Stellar [Fe/H] and the frequency of exo-Neptunes. *A&A* **487**, 373-381 (2008).
2. V. Adibekyan, S. G. Sousa, N. C. Santos, *Asteroseismology and Exoplanets: Listening to the Stars and Searching for New Worlds*, T. L. Campante, N. C. Santos, M. J. P. F. G. Monteiro, eds. (2018), vol. 49, p. 225.
3. B. J. Fulton, E. A. Petigura, A. W. Howard, H. Isaacson, G. W. Marcy, P. A. Cargile, L. Hebb, L. M. Weiss, J. A. Johnson, T. D. Morton, E. Sinukoff, I. J. M. Crossfield, L. A. Hirsch, The California-Kepler Survey. III. A Gap in the Radius Distribution of Small Planets. *AJ* **154**, 109 (2017).
4. J. E. Owen, Y. Wu, The Evaporation Valley in the Kepler Planets. *ApJ* **847**, 29 (2017).
5. S. Ginzburg, H. E. Schlichting, R. Sari, Core-powered mass-loss and the radius distribution of small exoplanets. *MNRAS* **476**, 759-765 (2018).
6. S. Jin, C. Mordasini, Compositional Imprints in Density-Distance-Time: A Rocky Composition for Close-in Low-mass Exoplanets from the Location of the Valley of Evaporation. *ApJ* **853**, 163 (2018).
7. J. Venturini, O. M. Guilera, J. Haldemann, M. P. Ronco, C. Mordasini, The Nature of the Radius Valley: Hints from Formation and Evolution Models. *arXiv e-prints* p. arXiv:2008.05513 (2020).
8. M. Asplund, N. Grevesse, A. J. Sauval, P. Scott, The Chemical Composition of the Sun. *ARA&A* **47**, 481-522 (2009).
9. J. C. Bond, D. P. O'Brien, D. S. Lauer, The Compositional Diversity of Extrasolar Terrestrial Planets. I. In Situ Simulations. *ApJ* **715**, 1050-1070 (2010).

10. A. Thiabaud, U. Marboeuf, Y. Alibert, N. Cabral, I. Leya, K. Mezger, From stellar nebula to planets: The refractory components. *A&A* **562**, A27 (2014).
11. A. Bonsor, P. Jofre, O. Shorttle, L. K. Rogers, S. Xu, C. Melis, Host-star and exoplanet compositions: a pilot study using a wide binary with a polluted white dwarf. *arXiv e-prints* p. arXiv:2102.02843 (2021).
12. C. Dorn, A. Khan, K. Heng, J. A. D. Connolly, Y. Alibert, W. Benz, P. Tackley, Can we constrain the interior structure of rocky exoplanets from mass and radius measurements? *A&A* **577**, A83 (2015).
13. C. T. Unterborn, E. E. Dismukes, W. R. Panero, Scaling the Earth: A Sensitivity Analysis of Terrestrial Exoplanetary Interior Models. *ApJ* **819**, 32 (2016).
14. K. Lodders, Solar System Abundances and Condensation Temperatures of the Elements. *ApJ* **591**, 1220-1247 (2003).
15. N. C. Santos, V. Adibekyan, C. Mordasini, W. Benz, E. Delgado-Mena, C. Dorn, L. Buchhave, P. Figueira, A. Mortier, F. Pepe, A. Santerne, S. G. Sousa, S. Udry, Constraining planet structure from stellar chemistry: the cases of CoRoT-7, Kepler-10, and Kepler-93. *A&A* **580**, L13 (2015).
16. N. C. Santos, V. Adibekyan, C. Dorn, C. Mordasini, L. Noack, S. C. C. Barros, E. Delgado-Mena, O. Demangeon, J. P. Faria, G. Israelian, S. G. Sousa, Constraining planet structure and composition from stellar chemistry: trends in different stellar populations. *A&A* **608**, A94 (2017).
17. W. F. McDonough, Compositional Model for the Earth's Core. *Treatise on Geochemistry* **2**, 568 (2003).
18. C. Dorn, J. Venturini, A. Khan, K. Heng, Y. Alibert, R. Helled, A. Rivoldini, W. Benz, A generalized Bayesian inference method for constraining the interiors of super Earths and sub-Neptunes. *A&A* **597**, A37 (2017).



19. S. Ulmer-Moll, N. C. Santos, P. Figueira, J. Brinchmann, J. P. Faria, Beyond the exoplanet mass-radius relation. *A&A* **630**, A135 (2019).
20. M. Plotnykov, D. Valencia, Chemical Fingerprints of Formation in Rocky Super-Earths' Data. *MNRAS* (2020).
21. A. Aguichine, O. Mousis, B. Devouard, T. Ronnet, Rocklines as Cradles for Refractory Solids in the Protosolar Nebula. *ApJ* **901**, 97 (2020).
22. J. G. Schulze, J. Wang, J. A. Johnson, C. T. Unterborn, W. R. Panero, The Probability that a Rocky Planet's Composition Reflects its Host Star. *arXiv e-prints* p. arXiv:2011.08893 (2020).
23. J. Lillo-Box, T. A. Lopez, A. Santerne, L. D. Nielsen, S. C. C. Barros, M. Deleuil, L. Acuña, O. Mousis, S. G. Sousa, V. Adibekyan, D. J. Armstrong, D. Barrado, D. Bayliss, D. J. A. Brown, O. D. S. Demangeon, X. Dumusque, P. Figueira, S. Hojjatpanah, H. P. Osborn, N. C. Santos, S. Udry, Masses for the seven planets in K2-32 and K2-233. Four diverse planets in resonant chain and the first young rocky worlds. *A&A* **640**, A48 (2020).
24. A. Mortier, *et al.*, K2-111: an old system with two planets in near-resonance. *MNRAS* (2020).
25. B. Bitsch, C. Battistini, Influence of sub- and super-solar metallicities on the composition of solid planetary building blocks. *A&A* **633**, A10 (2020).
26. A. Michel, J. Haldemann, C. Mordasini, Y. Alibert, Planetary mass-radius relations across the galaxy. *A&A* **639**, A66 (2020).
27. G. R. Ricker, *et al.*, Transiting Exoplanet Survey Satellite (TESS). *Journal of Astronomical Telescopes, Instruments, and Systems* **1**, 014003 (2015).
28. F. Pepe, *et al.*, ESPRESSO@VLT – On-sky performance and first results. *arXiv e-prints* p. arXiv:2010.00316 (2020).

29. W. Benz, *et al.*, The CHEOPS mission. *arXiv e-prints* p. arXiv:2009.11633 (2020).
30. H. Rauer, *et al.*, The PLATO 2.0 mission. *Experimental Astronomy* **38**, 249-330 (2014).
31. J. Schneider, C. Dedieu, P. Le Sidaner, R. Savalle, I. Zolotukhin, Defining and cataloging exoplanets: the exoplanet.eu database. *A&A* **532**, A79 (2011).
32. B. Toledo-Adr, *et al.*, Characterization of the K2-38 planetary system. Unraveling one of the densest planets known to date. *arXiv e-prints* p. arXiv:2007.01081 (2020).
33. S. M. Mills, T. Mazeh, The Planetary Mass-Radius Relation and Its Dependence on Orbital Period as Measured by Transit Timing Variations and Radial Velocities. *ApJ* **839**, L8 (2017).
34. N. R. Hinkel, P. A. Young, M. D. Pagano, S. J. Desch, A. D. Anbar, V. Adibekyan, S. Blanco-Cuaresma, J. K. Carlberg, E. Delgado Mena, F. Liu, T. Nordlander, S. G. Sousa, A. Korn, P. Gruyters, U. Heiter, P. Jofr N. C. Santos, C. Soubiran, A Comparison of Stellar Elemental Abundance Techniques and Measurements. *ApJS* **226**, 4 (2016).
35. P. E. Nissen, B. Gustafsson, High-precision stellar abundances of the elements: methods and applications. *A&A Rev.* **26**, 6 (2018).
36. P. Jofr U. Heiter, C. Soubiran, Accuracy and Precision of Industrial Stellar Abundances. *ARA&A* **57**, 571-616 (2019).
37. L. Ghezzi, K. Cunha, S. C. Schuler, V. V. Smith, Metallicities of Planet-hosting Stars: A Sample of Giants and Subgiants. *ApJ* **725**, 721-733 (2010).
38. E. Brugamyer, S. E. Dodson-Robinson, W. D. Cochran, C. Sneden, Silicon and Oxygen Abundances in Planet-host Stars. *ApJ* **738**, 97 (2011).
39. N. C. Santos, S. G. Sousa, A. Mortier, V. Neves, V. Adibekyan, M. Tsantaki, E. Delgado Mena, X. Bonfils, G. Israelian, M. Mayor, S. Udry, SWEET-Cat: A catalogue of parameters for Stars

- With ExoplanETs. I. New atmospheric parameters and masses for 48 stars with planets. *A&A* **556**, A150 (2013).
40. S. G. Sousa, V. Adibekyan, E. Delgado-Mena, N. C. Santos, D. T. Andreasen, A. C. S. Ferreira, M. Tsantaki, S. C. C. Barros, O. Demangeon, G. Israelian, J. P. Faria, P. Figueira, A. Mortier, I. Brandão, M. Montalto, B. Rojas-Ayala, A. Santerne, SWEET-Cat updated. New homogenous spectroscopic parameters. *A&A* **620**, A58 (2018).
41. V. Adibekyan, S. G. Sousa, N. C. Santos, P. Figueira, C. Allende Prieto, E. Delgado Mena, J. I. González Hernández, P. de Laverny, A. Recio-Blanco, T. L. Campante, M. Tsantaki, A. A. Hakobyan, M. Oshagh, J. P. Faria, M. Bergemann, G. Israelian, T. Boulet, Benchmark stars, benchmark spectrographs. Detailed spectroscopic comparison of ESPRESSO, PEPSI, and HARPS data for Gaia benchmark stars. *A&A* **642**, A182 (2020).
42. S. G. Sousa, *ARES + MOOG: A Practical Overview of an Equivalent Width (EW) Method to Derive Stellar Parameters* (2014), pp. Springer International Publishing (Cham), Edited by Ewa Niemczura, Barry Smalley and Wojtek Pych, pp. 297–310.
43. S. G. Sousa, N. C. Santos, V. Adibekyan, E. Delgado-Mena, G. Israelian, ARES v2: new features and improved performance. *A&A* **577**, A67 (2015).
44. R. L. Kurucz, *SYNTHÉ spectrum synthesis programs and line data* (1993).
45. C. A. Sneden, Carbon and Nitrogen Abundances in Metal-Poor Stars., Ph.D. thesis, THE UNIVERSITY OF TEXAS AT AUSTIN. (1973).
46. V. Z. Adibekyan, E. Delgado Mena, S. G. Sousa, N. C. Santos, G. Israelian, J. I. González Hernández, M. Mayor, A. A. Hakobyan, Exploring the  $\alpha$ -enhancement of metal-poor planet-hosting stars. The Kepler and HARPS samples. *A&A* **547**, A36 (2012).

47. V. Z. Adibekyan, S. G. Sousa, N. C. Santos, E. Delgado Mena, J. I. González Hernández, G. Israelian, M. Mayor, G. Khachatryan, Chemical abundances of 1111 FGK stars from the HARPS GTO planet search program. Galactic stellar populations and planets. *A&A* **545**, A32 (2012).
48. V. Adibekyan, P. Figueira, N. C. Santos, S. G. Sousa, J. P. Faria, E. Delgado-Mena, M. Oshagh, M. Tsantaki, A. A. Hakobyan, J. I. González Hernández, L. Suárez-Andrés, G. Israelian, Identifying the best iron-peak and  $\alpha$ -capture elements for chemical tagging: The impact of the number of lines on measured scatter. *A&A* **583**, A94 (2015).
49. E. Delgado Mena, G. Israelian, J. I. González Hernández, J. C. Bond, N. C. Santos, S. Udry, M. Mayor, Chemical Clues on the Formation of Planetary Systems: C/O Versus Mg/Si for HARPS GTO Sample. *ApJ* **725**, 2349-2358 (2010).
50. S. Bertran de Lis, E. Delgado Mena, V. Z. Adibekyan, N. C. Santos, S. G. Sousa, Oxygen abundances in G- and F-type stars from HARPS. Comparison of [OI] 6300 Å and OI 6158 Å. *A&A* **576**, A89 (2015).
51. F. Pedregosa, G. Varoquaux, A. Gramfort, V. Michel, B. Thirion, O. Grisel, M. Blondel, P. Prettenhofer, R. Weiss, V. Dubourg, J. Vanderplas, A. Passos, D. Cournapeau, M. Brucher, M. Perrot, Édouard Duchesnay, Scikit-learn: Machine learning in python. *Journal of Machine Learning Research* **12**, 2825-2830 (2011).
52. E. Delgado Mena, M. Tsantaki, V. Z. Adibekyan, S. G. Sousa, N. C. Santos, J. I. González Hernández, G. Israelian, Chemical abundances of 1111 FGK stars from the HARPS GTO planet search program. II. Cu, Zn, Sr, Y, Zr, Ba, Ce, Nd, and Eu. *A&A* **606**, A94 (2017).
53. E. Caffau, H. G. Ludwig, P. Bonifacio, R. Faraggiana, M. Steffen, B. Freytag, I. Kamp, T. R. Ayres, The solar photospheric abundance of carbon. Analysis of atomic carbon lines with the CO5BOLD solar model. *A&A* **514**, A92 (2010).

54. E. Caffau, H. G. Ludwig, M. Steffen, T. R. Ayres, P. Bonifacio, R. Cayrel, B. Freytag, B. Plez, The photospheric solar oxygen project. I. Abundance analysis of atomic lines and influence of atmospheric models. *A&A* **488**, 1031-1046 (2008).
55. Gaia Collaboration, VizieR Online Data Catalog: Gaia DR2 (Gaia Collaboration, 2018). *VizieR Online Data Catalog* p. I/345 (2018).
56. P. J. Flower, Transformations from Theoretical Hertzsprung-Russell Diagrams to Color-Magnitude Diagrams: Effective Temperatures, B-V Colors, and Bolometric Corrections. *ApJ* **469**, 355 (1996).
57. E. Agol, C. Dorn, S. L. Grimm, M. Turbet, E. Ducrot, L. Delrez, M. Gillon, B.-O. Demory, A. Burdanov, K. Barkaoui, *et al.*, Refining the transit timing and photometric analysis of trappist-1: Masses, radii, densities, dynamics, and ephemerides. *arXiv preprint arXiv:2010.01074* (2020).
58. K. Hakim, A. Rivoldini, T. Van Hoolst, S. Cottenier, J. Jaeken, T. Chust, G. Steinle-Neumann, A new ab initio equation of state of hcp-Fe and its implication on the interior structure and mass-radius relations of rocky super-Earths. *Icarus* **313**, 61-78 (2018).
59. C. Sotin, O. Grasset, A. Mocquet, Mass-radius curve for extrasolar earth-like planets and ocean planets. *Icarus* **191**, 337-351 (2007).
60. J. Monteux, G. J. Golabek, D. C. Rubie, G. Tobie, E. D. Young, Water and the interior structure of terrestrial planets and icy bodies. *Space Science Reviews* **214**, 1-33 (2018).
61. A. E. Doyle, E. D. Young, B. Klein, B. Zuckerman, H. E. Schlichting, Oxygen fugacities of extra-solar rocks: Evidence for an Earth-like geochemistry of exoplanets. *Science* **366**, 356-359 (2019).
62. K. Hakim, A. Rivoldini, T. Van Hoolst, S. Cottenier, J. Jaeken, T. Chust, G. Steinle-Neumann, A new ab initio equation of state of hcp-Fe and its implication on the interior structure and mass-radius relations of rocky super-Earths. *Icarus* **313**, 61-78 (2018).

63. L. Wang, F. Dai, Evaporation of Low-mass Planet Atmospheres: Multidimensional Hydrodynamics with Consistent Thermochemistry. *ApJ* **860**, 175 (2018).
64. P. Figueira, J. P. Faria, V. Z. Adibekyan, M. Oshagh, N. C. Santos, A Pragmatic Bayesian Perspective on Correlation Analysis. The exoplanetary gravity - stellar activity case. *Origins of Life and Evolution of the Biosphere* **46**, 385-393 (2016).
65. G. Gonzalez, The stellar metallicity-giant planet connection. *MNRAS* **285**, 403-412 (1997).
66. N. C. Santos, G. Israelian, M. Mayor, The metal-rich nature of stars with planets. *A&A* **373**, 1019-1031 (2001).
67. C. D. Dressing, D. Charbonneau, X. Dumusque, S. Gettel, F. Pepe, A. Collier Cameron, D. W. Latham, E. Molinari, S. Udry, L. Affer, A. S. Bonomo, L. A. Buchhave, R. Cosentino, P. Figueira, A. F. M. Fiorenzano, A. Harutyunyan, R. D. Haywood, J. A. Johnson, M. Lopez-Morales, C. Lovis, L. Malavolta, M. Mayor, G. Micela, F. Motalebi, V. Nascimbeni, D. F. Phillips, G. Piotto, D. Pollacco, D. Queloz, K. Rice, D. Sasselov, D. Sgransan, A. Sozzetti, A. Szentgyorgyi, C. Watson, The Mass of Kepler-93b and The Composition of Terrestrial Planets. *ApJ* **800**, 135 (2015).

## Acknowledgments

This work was supported by FCT - Fundação para a Ciência e Tecnologia (FCT) through national funds and by FEDER through COMPETE2020 - Programa Operacional Competitividade e Internacionalização by these grants: UID/FIS/04434/2019; UIDB/04434/2020; UIDP/04434/2020; PTDC/FIS-AST/32113/2017 & POCI-01-0145-FEDER-032113; PTDC/FIS-AST/28953/2017 & POCI-01-0145-FEDER-028953. V.A., E.D.M, N.C.S., and S.G.S. also acknowledge the support from FCT through Investigador FCT contracts nr. IF/00650/2015/CP1273/CT0001, IF/00849/2015/CP1273/CT0003, IF/00169/2012/ and IF/00028/2014/CP1215/CT0002, respectively, and POPH/FSE (EC) by FEDER funding through the program “Programa Operacional de Factores de Competitividade - COMPETE”. C.D. acknowledges support from the Swiss National Science Foundation under grant PZ00P2\_174028, this work has been carried out within the frame of the National Center for Competence in Research PlanetS supported by the SNSF. O.D.S.D. and J.P.F. are supported in the form of work contracts (DL 57/2016/CP1364/CT0004 and DL57/2016/CP1364/CT0005, respectively) funded by FCT. E.M. acknowledge funding from the French National Research Agency (ANR) under contract number ANR-18-CE31-0019 (SPLaSH). B.B., thanks the European Research Council (ERC Starting Grant 757448-PAMDORA) for their financial support. Based on observations (program ID GN-217A-FT-20; PI: E. Jofre) obtained at the international Gemini Observatory, a program of NSF’s NOIRLab, which is managed by the Association of Universities for Research in Astronomy (AURA) under a cooperative agreement with the National Science Foundation on behalf of the Gemini Observatory partnership: the National Science Foundation (United States), National Research Council (Canada), Agencia Nacional de Investigación y Desarrollo (Chile), Ministerio de Ciencia, Tecnología e Innovación (Argentina), Ministério da Ciência, Tecnologia, Inovações e Comunicações (Brazil), and Korea Astronomy and Space Science Institute (Republic of Korea). This work has made use of data from the European Space Agency (ESA) mission (Gaia), processed by the Gaia Data Processing and Analysis Consortium (dpac). Funding for the dpac has been provided by national institutions, in particular the institutions

participating in the Gaia Multilateral Agreement. In this work we used the Python language and several scientific packages. **Author contributions:** V.A. led the data analysis and wrote the paper with contribution of C.D.. C.D. led the planetary interior analysis and S.G.S. performed the stellar parameter analysis. V.A. determined the chemical composition of the stars with contribution of E.D.M., N.C.S., B.B., C.M., and G.I. contributed to the discussion of the implications of the data. S.C.C.B., O.D.S.D., A.A.H, M.O. contributed to the general discussion of the results. C.D, S.G.S, N.C.S., G.I., C.M., E.D.M., M.K., Y.T., E.J., R.P., and E.M. worked on gathering the spectroscopic observations. J.P.F. and P.F. contributed to the statistical analysis. All authors discussed the results and commented on the manuscript. **Competing interests:** The authors declared no competing interests. **Data and materials availability:** The data supporting the findings of this study are available within the paper and its supplementary tables. The combined spectra of the planet host stars are available upon reasonable request from the corresponding author. The main analysis routines have been written by the authors and are available upon reasonable request from the corresponding author. The latest version of ARES code (ARES v2) is available at <http://www.astro.up.pt/~sousasag/ares>. BayesCorr code is freely available for download or cloning in the git repository <https://bitbucket.org/pedrofigueira/bayesiancorrelation/>



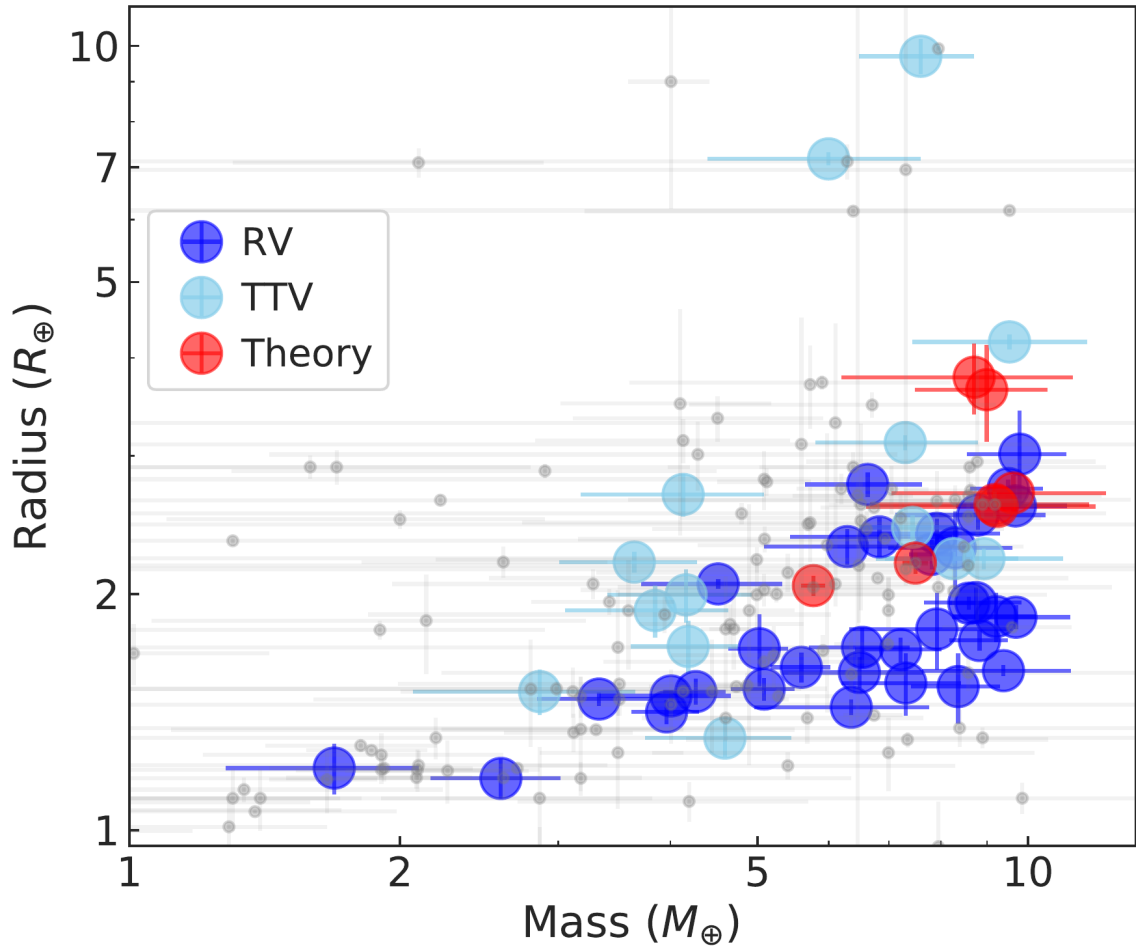


Figure 1: **Radius-mass diagram.** Distribution of low-mass planets (masses below  $10 M_{\oplus}$ ) with precise mass and radius measurements or estimates (uncertainties below 30%) in the R-M diagram (<http://exoplanet.eu>, on 11th May 2020). Mass determination methods are indicated by different colors. Grey points indicate the planets with imprecise (uncertainties above 30%) mass or radius estimates. All error bars show one standard deviation.

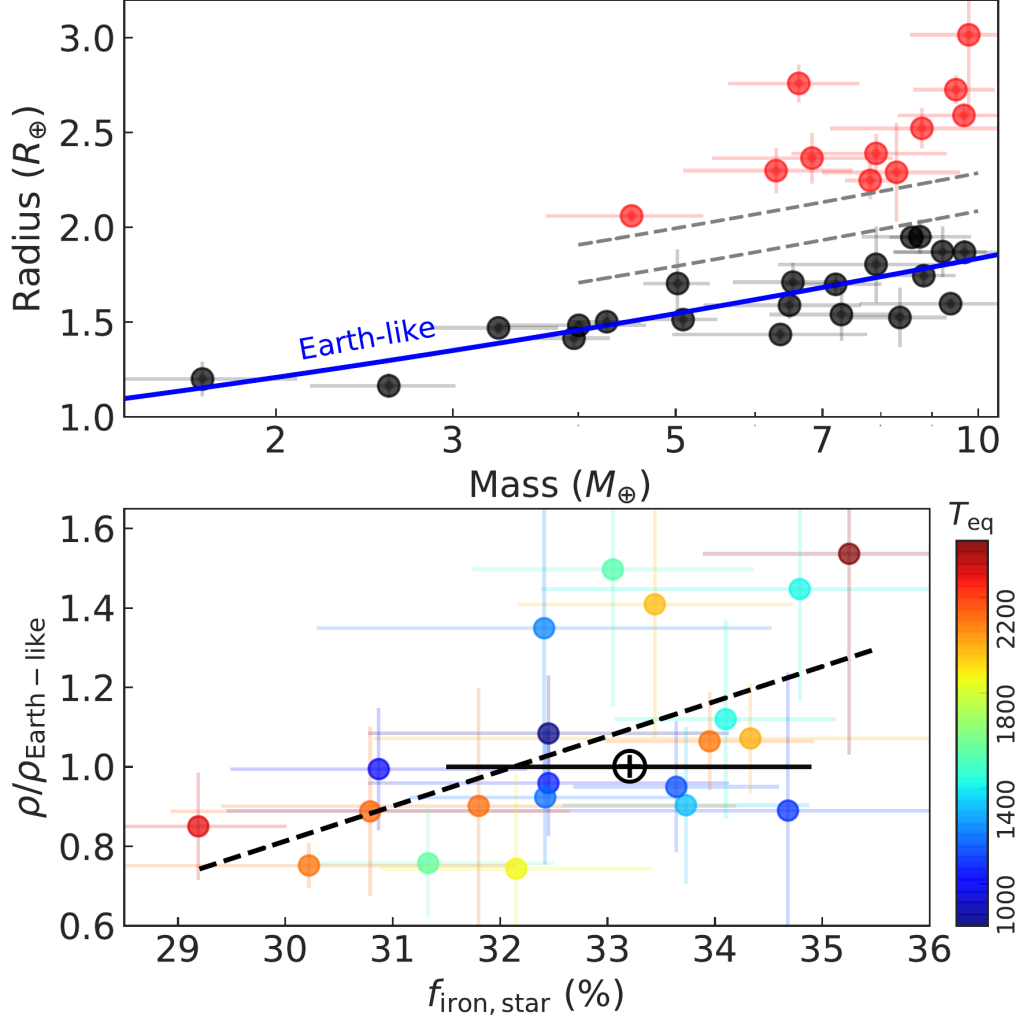


Figure 2: **Densities of rocky planets.** Top panel. Mass-radius diagram for RV-detected planets with masses below  $10 M_{\oplus}$  for which the uncertainty both in mass and radius is below 30%. The grey dashed curves, drawn by eye, indicate the location of the 'radius gap' which separates the planets into planets with (red circles) and without (black circles) envelopes. The blue curve shows the mass-radius relationship for Earth-like composition (32% Fe + 68% MgSiO<sub>3</sub>) (18). Bottom panel. Normalized density of the planets as a function of iron mass fraction of planet building blocks estimated from the host star chemistry.  $\rho_{\text{Earth-like}}$  is the density of a planet with Earth-like composition for a given mass. The black dashed line represent the results of the OLS linear regression. The position of the Earth is indicated with its symbol in black. The symbols are color-coded by the equilibrium temperature of the planets. All error bars show one standard deviation.

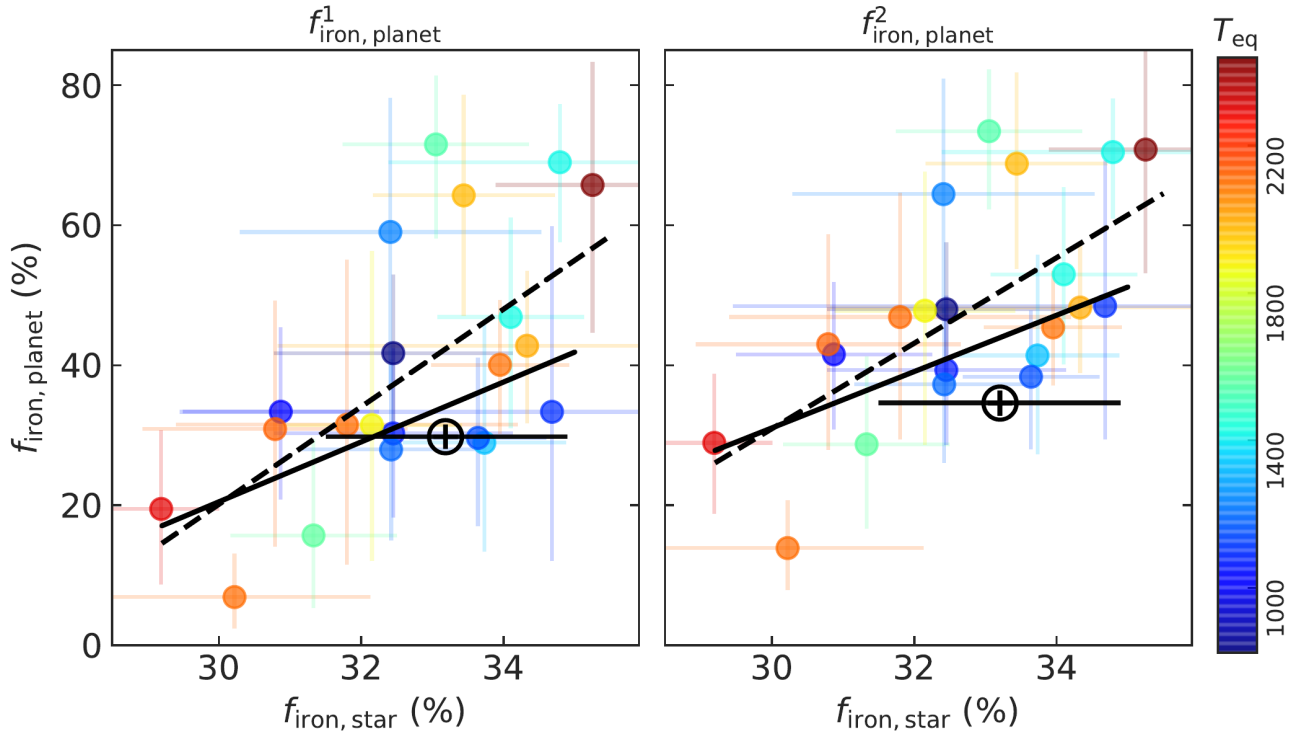


Figure 3: **Iron content in rocky planets.** Iron mass fraction of planet building blocks estimated from the host star chemistry ( $f_{\text{iron,star}}$ ) versus iron mass fraction from the planets ( $f_{\text{iron,planet}}$ ) as estimated by mass and radius and using a detailed interior model (18). Estimates of  $f_{\text{iron,planet}}$  are based on the assumption that all iron resides in the core only (left panel) or iron is assumed to be present in both mantle and core (right panel). The symbols are color-coded by the equilibrium temperature of the planets. The black dashed and solid lines represent the results of the OLS linear regression for the full sample and for the sample of planets without considering the five planets with the highest  $f_{\text{iron,planet}}$ , respectively. The positions of the Earth are indicated with its symbol in black. The error bars of  $f_{\text{iron,star}}$  show one standard deviation. The error bars of  $f_{\text{iron,planet}}$  cover the interval between the 16th and the 84th percentiles.

## Materials and Methods

### The sample

We started our sample selection from exoplanet.eu (31). Out of 4330 confirmed planets (as of 11/05/2020) 364 turned out to have masses below  $10 M_{\oplus}$  and to orbit around FGK-type stars ( $4500 < T_{\text{eff}} < 6500$  K). We further selected 56 well-characterized planets defined by having a precision in both mass and radius better than 30%. To this sample we added the recently characterized planetary system K2-38, consisting of two low-mass planets (32). The distribution of these planets on the mass-radius diagram along with the method of the mass determination is shown in the top panels of Fig.1.

From this sample we then excluded all planets with mass estimations based on mass-radius empirical relation (indicated as “Theory” in Fig.1) and planets with mass determination based on the TTV method. As already discussed in the literature (33) and also can be seen in Fig.1 the planets with TTV- and RV-based masses determinations (hereinafter referred to as TTV-planets and RV-planets) show different distributions in the diagram. Because of this still to-be-understood difference we limit our sample to 33 RV-planets (in 27 planetary systems) only.

### Stellar parameters and chemical abundances

Paramount to the analysis of star-planet relations is our ability to derive precise stellar parameters and chemical abundances for planet host stars. Many groups all over the world are working intensively to push down the precision limits in deriving fundamental properties and chemical abundances of planet host stars (2, 34–36). The general conclusion is that in most cases exoplanet host stars can be very precisely characterized if their spectral analysis is done homogeneously (37–39).

For the sample of 26 planet host stars we collected high-resolution optical spectra from public archives (ESO, HARPS-N@TNG, SOPHIE@OHP, ESPaDOnS@CFHT, HIRES@Keck) and through dedicated observing programs carried out by the authors (GRACES@Gemini-N, ESPRESSO@VLT, and HDS@Subaru). Unfortunately, for one of the stars (HD 80653) we were not able to get a high-

resolution spectrum and we had to exclude this star from our sample. It is important to note that with the spectroscopic analysis adopted in this work the impact of using different instruments is very small (40, 41).

We determined the stellar atmospheric parameters ( $T_{\text{eff}}$ ,  $\log g$ , microturbulence ( $V_{\text{mic}}$ ), and  $[\text{Fe}/\text{H}]$ ) of the sample stars following the methodology described in (39, 42). We make use of the equivalent widths (EW) of iron lines, as measured in the combined spectra using the ARES v2 code (43), and we assume ionization and excitation equilibrium. The process makes use of a grid of Kurucz model atmospheres (44) and the 2014 version of the radiative transfer code MOOG (45).

For K2-216, with a  $T_{\text{eff}}$  of  $\sim 4500$  K, the microturbulent velocity was close to zero, which is unrealistically small. For this star we determined the microturbulence using the empirical calibration from (46).

Stellar abundances of the elements were also derived using the same tools and models as for stellar parameter determination, as well as using the classical curve-of-growth analysis method assuming local thermodynamic equilibrium. Although the EWs of the spectral lines were automatically measured with ARES, for the elements with only two-three lines available we performed careful visual inspection of the EWs measurements. For the derivation of chemical abundances of refractory elements we closely followed the methods described in (47, 48). Abundances of the volatile elements, O and C, were derived following the method of (49, 50). The EWs of the spectral lines of C, O, and Mg were manually measured with the task `splot` in IRAF.

C and O abundances are very difficult to determine for stars cooler than about 5200 K (49, 50). We could not determine C abundance for 4 of the stars and O abundance for 6 stars. For the aforementioned stars we estimated the abundances of C and O empirically by using a machine learning algorithm (we used the estimator "RandomForestRegressor") from the Python Scikit-learn package (51). The estimation of C and O was based on the abundance of Mg and Fe (52). Our initial sample was based on the HARPS sample (47). We derived O abundance for 535 stars and C abundance of 758 stars following the methodology of our previous works (49, 50). These samples were used as training and test datasets.

The average error for the estimated C and O abundances are 0.08 and 0.09 dex respectively. We tested the estimated C and O abundances for our sample of planet host stars for which we determined the abundances of these elements. The mean difference and standard deviation for C and O are  $-0.01 \pm 0.06$  and  $-0.04 \pm 0.10$  dex, respectively.

The final stellar parameters and chemical abundances of the sample stars are presented in Supplementary Table 1. Note that the abundances listed in the table are relative to the Sun.

We used the atmospheric abundances of C, O, Mg, Si, and Fe to estimate the  $f_{\text{iron,star}}$  (15, 16). To do so, we needed to transform the relative abundances into absolute abundances considering solar reference values. The solar absolute abundances were taken as  $\log \epsilon_{\text{C}} = 8.5$  (53),  $\log \epsilon_{\text{O}} = 8.65$  (54),  $\log \epsilon_{\text{Mg}} = 7.6$  (8),  $\log \epsilon_{\text{Si}} = 7.51$  (8), and  $\log \epsilon_{\text{Fe}} = 7.5$  (8). It is important to note that the  $f_{\text{iron,star}}$  is practically insensitive to the abundances of C and O. For example varying the C and O abundances by 0.2 dex introduces an average variation of only 0.02% in  $f_{\text{iron,star}}$ , which is by a factor of 25 smaller than the average relative uncertainty of  $f_{\text{iron,star}}$ .

The luminosity of the planet host stars was calculated by using spectroscopic effective temperature, V magnitude, Gaia DR2 parallax (55), and bolometric correction (56).

## Physical properties of the rocky planets

The main source for the planetary parameters was exoplanet.eu. We computed the bulk density,  $\rho$ , of the planets based on their mass and radius. Since planets with the same composition but with different masses would have different bulk densities, we scaled the densities to the density of a planet with Earth-like composition (18) for a given mass -  $\rho_{\text{Earth-like}}$ .

Given the planet's mass and radius, we estimated their possible iron fraction  $f_{\text{iron,planet}}$ , which is defined as  $(M_{\text{Fe,mantle}} + M_{\text{core}})/M_{\text{pl}}$ , where  $M_{\text{Fe,mantle}}$  and  $M_{\text{core}}$  are the masses of iron in mantle and core, respectively. In addition, we also estimated the possible Fe/(Mg+Si) abundance ratio of the planets. We used an interior model as in (57) and a characterization scheme as in (18) that employs a Markov chain Monte Carlo (McMC) method. For the planet interiors, we assume a pure iron core and a

silicate mantle, and neglect any volatile layers. The interior model uses self-consistent thermodynamics in the core and mantle. For the core, we use the equations of state for hexagonal close packed iron (58) and for the silicate mantle we use the model from (59). We assume an adiabatic temperature profile within core and mantle.

When estimating  $f_{\text{iron,planet}}$ , we test two scenarios: First, we only allow the core to vary in size and fix the iron content of the mantle at zero (Fig. 3, left panel). In a second scenario, we also allow the mantle composition to vary in iron content (Fig. 3, right panel). This results in  $\sim 10\%$  higher  $f_{\text{iron,planet}}$ , since high amounts of iron can be in part compensated by high amounts of oxygen to fit the same mass and radius data. Average estimated Mg-numbers of the mantles ( $\text{Mg}/(\text{Mg}+\text{Fe})$ ) range from 0.45 to 0.9 with large uncertainties of up to 60%. And this may bolster the long-range migration scenario in which the planets formed in a highly oxidizing environment which enabled the iron to remain in the mantle (60). These models have average oxygen fugacities  $-3$  to  $-1.7\Delta\text{IW}^1$  which is comparable to the oxidation state of Earth, small bodies, both in our solar system and accreted by white dwarfs (61).

In our analysis we neglected light elements in the core, since their addition has only tiny effects on the total radius. For example, we find that for a fixed Fe/Si bulk ratio, the addition of light alloys like  $\text{Fe}_{0.95}\text{O}$  in the core only affects the radius by 0.2%, when using the recent light alloy equations of state data (62).

The  $T_{\text{eq}}$  of the exoplanets were computed using the stellar luminosity and orbital distances of the planets assuming zero bond albedo (63). Semi-major axis for K2-141 b and Kepler-406 b, however, were not available in the exoplanet.eu and were extracted from <http://exoplanets.org> and <http://exoplanetarchive.ipac.caltech.edu/> respectively.

The parameters of the rocky planets are presented in Suplimentary Table 2.

---

<sup>1</sup>Oxygen fugacity is defined relative to the Iron-Wüstite equilibrium reaction  $\text{Fe}+0.5\text{O}_2=\text{FeO}$  (Wüstite) such that  $\Delta\text{IW} = \log(f_{\text{O}_2})_{\text{rock}} - \log(f_{\text{O}_2})_{\text{IW}}$

## Significance and robustness of the results

We performed several frequentist and Bayesian tests to assess the significance of the observed planet density –  $f_{\text{iron,star}}$  and  $f_{\text{iron,planet}} - f_{\text{iron,star}}$  correlations. When performing the tests besides the main sample we also considered a sub-sample of 18 planets with uncertainties both in mass and radius below 20%. The results of our tests are summarized in Suplimentary Table 3.

We first performed an ordinary least squares (OLS) and weighted least squares (WLS) regression to quantify the  $\rho/\rho_{\text{Earth-like}}$  vs  $f_{\text{iron,star}}$  and  $f_{\text{iron,planet}} - f_{\text{iron,star}}$  correlations. The inverse of variance ( $\sigma^2$ ) of the planet density and  $f_{\text{iron,planet}}$  were, respectively, used to calculate the weights. The p-values (at  $\alpha = 0.05$  significance level) come from the F-statistics that tests the null hypothesis that the data can be modeled accurately by setting the regression coefficients to zero. The p-values vary from 0.007 to  $1 \times 10^{-5}$ , indicating that the observed correlations are significant. It is also evident that the p-values are overall smaller for the sub-sample of more precisely characterized planets.

We also performed two simple Monte Carlo (MC) tests to access the significance of the observed correlations. In the first bootstrapped Monte Carlo test (MC I), for each correlation we estimated the Spearman's rank (Spearman's  $\rho$ ) correlation coefficient which are presented in the Table. Then we shuffled the data points (random re-sampling with replacement) and calculated the corresponding the Spearman's  $\rho$ . We repeated the entire process  $10^5$  times and counted the number of trials in which the Spearman's  $\rho$  is equal to or larger than the correlation coefficient obtained for the original dataset. The results of this test, presented in Suplimentary Table 3, clearly show that the probability that the observed correlations have happened by a random alignment of this specific data set is always below 0.2%, i.e., larger than  $3\text{-}\sigma$ , if a normal distribution of alpha is assumed.

The second Monte Carlo (MC II) test was designed to consider the uncertainties in the parameters. For each correlation we created  $10^5$  mock samples by varying the parameters within their uncertainties assuming a normal distribution. Then for each of the sample we calculated the Spearman's rank (Spearman's  $\rho$ ) correlation coefficient. In Suplimentary Table 3 we present the fraction of cases when the Spearman's  $\rho$  has a negative value ( $P(\text{Sp. } \rho < 0)$  in the Table) i.e. opposite to what we expect if



the correlation is real. The table suggests that the probabilities that the observed positive correlations are influenced by the uncertainties varies from 2 to 5 percent depending on the sample and correlation. Again, significance is higher when considering the sub-sample of the best characterized planets.

Finally, we used the BayesCorr (64) code based on a Bayesian approach to assess the significance of a dependence of  $\rho/\rho_{\text{Earth-like}}$ ,  $f_{\text{iron,planet}}^1$ , and  $f_{\text{iron,planet}}^2$  on  $f_{\text{iron,star}}$  by calculating the Spearman’s rank correlation coefficient. This method, unfortunately does not consider the impact of the uncertainties on the measurements. In Table 3 we present the mean and standard deviation of Spearman’s  $\rho$ , as well as the associated 95% credible intervals (highest posterior density; HPD). The results show that the significance of the correlations vary from about  $3.4\text{-}\sigma$  to  $4.8\text{-}\sigma$ . As in the previous two tests the correlation is of higher significance when considering the sub-sample of the best characterized planets.

The four tests described in this section confirm that there is indeed a correlation between planetary density, iron-mass fraction of planets, and iron-mass fraction of planet building blocks. The fact that the correlations always become statistically more significant for the most precisely characterized planets further points towards the robustness of the observed trends.

Since the planetary parameters used in this work are not determined homogeneously, but taken from <http://exoplanet.eu> we performed another test to explore further how robust are our results to the heterogeneity in the planet data. From the NASA Exoplanet Archive (<https://exoplanetarchive.ipac.caltech.edu/>) we selected up to three latest published planetary parameters which satisfy the 30% relative uncertainty threshold we adopted in this work. For majority of the planets only one or two measurements were available in the aforementioned database, while for a few planets (e.g. Kepler-78 b and 55 Cnc e) literature is rich in measurements. For 55 Cnc e, we ignored the old measurements that lead to radius estimates above  $2R_{\oplus}$ , because in these cases the planet would lie above the radius gap and would not be included in the sample. We then considered all the possible combinations ( $\sim 4500$  realizations) of the planetary parameters (given the available planetary parameters for each system) performed OLS and WLS regressions to quantify the  $\rho/\rho_{\text{Earth-like}}$  vs  $f_{\text{iron,star}}$  correlation. In addition, we calculated the Spearman’s rank for each realization. This test

showed that the P(F-stat) values both for the OLS and WLS regressions are always smaller than 0.05 with the mean values being 0.01 and 0.004 for the OLS and WLS analysis, respectively. The values of Spearman's  $\rho$  lied in between 0.44 and 0.71, with a mean value of  $0.60 \pm 0.05$ . The results of this test confirm the statistical significance of our results and shows that they are robust to the various sources of planetary parameters.

## Super-Earths and super-Mercuries

As discussed in the manuscript and as can be seen in Fig. 3 the planets of our sample can be tentatively separate into super-Mercuries and super-Earths, where super-Mercuries are the planets with the highest  $f_{\text{iron,planet}}$ . For the sample of super-Earths we performed the main statistical tests discussed in the previous section. The results of our tests are presented in Supplementary Table 4. Most of the tests show that the relation between  $f_{\text{iron,planet}}$  and  $f_{\text{iron,star}}$  is statistically significant, although the level of significance is lower than when considering the full sample. This is both because the planets with the highest  $f_{\text{iron,planet}}$  are excluded and because the size of the sample is reduced by about 25%.

In Fig. 4 we show the dependence of Fe/(Mg+Si) abundance ratio of the planets on the same abundance ratio derived for the host stars. The super-Earths and super-Mercuries can be clearly identified in this plot. While, the sample of super-Mercuries is small and it is not possible to conclude whether a correlation exist for these planets, the sample of super-Earths clearly reveal a strong correlation. The p-values of the OLS and WLS analysis range from 0.005 to  $6 \times 10^{-5}$ , indicating that the observed correlations are significant.

We also performed an orthogonal distance regression analysis to quantify the  $Fe/(Mg + Si)_{\text{star}} - Fe/(Mg + Si)_{\text{planet}}$  relation considering uncertainties of both variables. The results are different for the two assumptions we made about the iron content in the planet:

$$Fe/(Mg + Si)_{\text{planet}}^1 = -1.82(\pm 0.48) + 5.33(\pm 1.17) \times Fe/(Mg + Si)_{\text{star}}$$

$$Fe/(Mg + Si)_{\text{planet}}^2 = -2.36(\pm 0.64) + 7.27(\pm 1.57) \times Fe/(Mg + Si)_{\text{star}}$$

where  $Fe/(Mg + Si)_{\text{planet}}^1$  and  $Fe/(Mg + Si)_{\text{planet}}^2$  correspond to the cases when iron is allowed to be only in the core, and in the core and mantle of planets, respectively. In both cases, however, the relation is not 1-to-1, which was typically assumed in the literature.

## Relation to previous works

Detection of only a few giant planets was required to notice that presence of these planets correlates with stellar metallicity (65, 66). Since these pioneering works, different research groups tried to link the chemical composition of stars with the properties of planets. With the increased precision of mass and radius of planets, it became possible to characterize the bulk composition of low-mass exoplanets. On a sample of five well-characterized planets with masses below  $6 M_{\oplus}$  it was shown that these low-mass planets can be characterized with a fixed ratio of iron to magnesium silicate corresponding to the value for the Earth (67). Immediately, the hypothesis that the hosts of these planets should have similar compositions was tested on a sample of three stars (15). While the later results (15) provided some hints that the iron mass fraction of planets is compatible with that inferred from the host star composition, making a general and firm conclusion was not possible because of the small sample size. Very recently, two interesting articles have been published performing a direct comparison of the composition of individual planets with the composition of their host stars (20, 22) and comparing the overall distribution of planet composition with the overall composition of planet host stars (20).

The approach adopted in this work is fundamentally different from the previous approaches in several aspects. 1) Performing a direct comparison of individual star-planet compositions is anti-sensitive to the precision of the planet and host star properties, meaning that the large uncertainties in the compositions of planets and stars will naturally lead to a similar composition at a low  $\sigma$ -level. 2) Since the typical uncertainties in planetary compositions are significantly larger than those determined from the host star abundances (22) (compare also Supplementary Table 1 and 2), one can underestimate the importance of the high-precision chemical characterization of planet host stars (22). 3) Finally, comparing compositions of individual planet-star system, makes difficult to infer general conclusions about

the relation and form of relation between compositions of stars and their planets.

Opposite to this, our approach was to statistically compare the composition of planets and their host stars. In our approach, high precision and homogeneity in compositions of both stars and planets is highly crucial. As a result, our approach allowed us to reach to a general conclusion that the iron mass fraction of planets correlates with the iron mass fraction of planet building blocks as inferred from the host star composition, and that this relation is not 1-to-1.

## Suplimentary Tables and Figures

Table 1: **Table S1 | Properties of the host stars.**

Star	$T_{\text{eff}}$ [K]	$\log g$ [dex]	Vtur [cgs]	[Fe/H]	[C/H]	[O/H]	[Mg/H]	[Si/H]	$f_{\text{iron,star}}$ [%]
------	----------------------	----------------	------------	--------	-------	-------	--------	--------	----------------------------

Table 2: **Table S2 | Properties of the rocky planets.**

Planet	R [ $R_{\oplus}$ ]	M [ $M_{\oplus}$ ]	Semi-major axis [AU]	$T_{\text{eq}}$ [K]	$\rho/\rho_{\text{Earth-like}}$	$f_{\text{iron,planet}}^1$ [%]	$f_{\text{iron,planet}}^2$ [%]
--------	--------------------	--------------------	----------------------	---------------------	---------------------------------	--------------------------------	--------------------------------

Table 3: **Table S3 | Results of the statistical tests.**

Data	OLS		WLS		MCI		MC II	Bayesian	
	Slope $\pm\sigma$	P(F-stat)	Slope $\pm\sigma$	P(F-stat)	Sp. $\rho^{\text{orig}}$	P(Sp. $\rho \geq \rho^{\text{orig}}$ )	P(Sp. $\rho \leq 0$ )	Sp. $\rho \pm \sigma$	95% HPD
$\rho/\rho_{\text{Earth-like}}$ vs $f_{\text{iron,star}}$ (30% precision)	0.09 $\pm$ 0.03	0.007	0.08 $\pm$ 0.02	1 $\times$ 10 <sup>-4</sup>	0.63	0.001	0.047	0.55 $\pm$ 0.14	[0.27, 0.81]
$\rho/\rho_{\text{Earth-like}}$ vs $f_{\text{iron,star}}$ (20% precision)	0.10 $\pm$ 0.03	0.002	0.08 $\pm$ 0.02	2 $\times$ 10 <sup>-4</sup>	0.72	4 $\times$ 10 <sup>-4</sup>	0.027	0.63 $\pm$ 0.13	[0.36, 0.85]
$f_{\text{iron,planet}}^1$ vs $f_{\text{iron,star}}$ (30% precision)	6.97 $\pm$ 1.96	0.002	9.20 $\pm$ 1.65	2 $\times$ 10 <sup>-5</sup>	0.60	0.002	0.026	0.52 $\pm$ 0.15	[0.22, 0.79]
$f_{\text{iron,planet}}^1$ vs $f_{\text{iron,star}}$ (20% precision)	7.52 $\pm$ 1.83	8 $\times$ 10 <sup>-4</sup>	8.96 $\pm$ 1.47	1 $\times$ 10 <sup>-5</sup>	0.67	0.002	0.017	0.57 $\pm$ 0.15	[0.27, 0.84]
$f_{\text{iron,planet}}^2$ vs $f_{\text{iron,star}}$ (30% precision)	6.11 $\pm$ 1.66	0.001	8.49 $\pm$ 1.50	2 $\times$ 10 <sup>-5</sup>	0.63	0.001	0.050	0.55 $\pm$ 0.14	[0.27, 0.79]
$f_{\text{iron,planet}}^2$ vs $f_{\text{iron,star}}$ (20% precision)	6.45 $\pm$ 1.62	0.001	8.24 $\pm$ 1.34	2 $\times$ 10 <sup>-5</sup>	0.66	0.002	0.037	0.57 $\pm$ 0.15	[0.26, 0.82]

Table 4: Table S4 | Results of the statistical tests for Super Earths.

Data	OLS		WLS		MC I		MC II	Bayesian	
	Slope $\pm\sigma$	P(F-stat)	Slope $\pm\sigma$	P(F-stat)	Sp. $\rho^{orig}$	P(Sp. $\rho \geq \rho^{orig}$ )	P(Sp. $\rho \leq 0$ )	Sp. $\rho \pm \sigma$	95% HPD
$f_{iron,planet}^1$ vs $f_{iron,star}$ (30% precision)	4.27 $\pm$ 1.24	0.005	6.66 $\pm$ 1.27	1 $\times$ 10 $^{-4}$	0.60	0.007	0.128	0.49 $\pm$ 0.17	[0.14, 0.79]
$f_{iron,planet}^1$ vs $f_{iron,star}$ (20% precision)	4.84 $\pm$ 1.39	0.004	6.82 $\pm$ 1.37	3 $\times$ 10 $^{-4}$	0.64	0.007	0.095	0.52 $\pm$ 0.18	[0.15, 0.83]
$f_{iron,planet}^2$ vs $f_{iron,star}$ (30% precision)	4.02 $\pm$ 1.23	0.005	5.55 $\pm$ 1.29	7 $\times$ 10 $^{-4}$	0.65	0.003	0.135	0.55 $\pm$ 0.16	[0.23, 0.83]
$f_{iron,planet}^2$ vs $f_{iron,star}$ (20% precision)	4.24 $\pm$ 1.36	0.009	5.62 $\pm$ 1.38	0.001	0.63	0.001	0.104	0.52 $\pm$ 0.18	[0.14, 0.81]

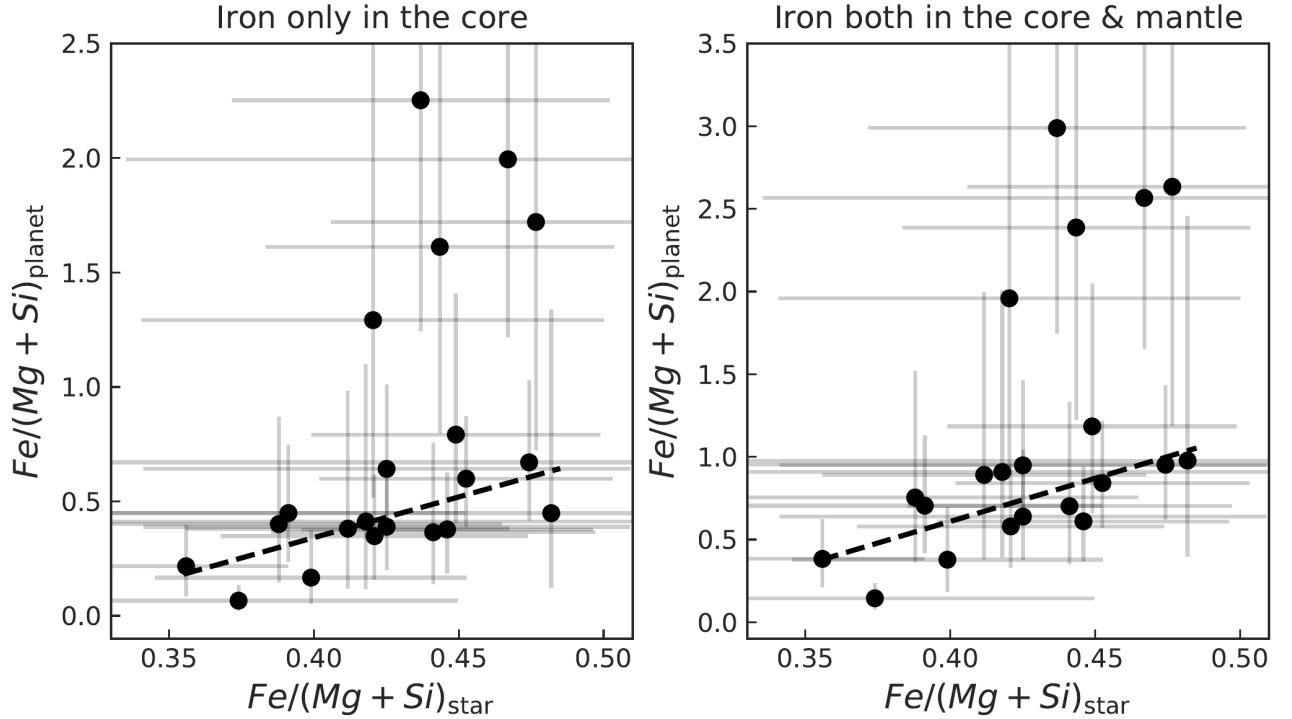


Figure 4: **Abundance ratios in planets and their hosts.** Fe/(Mg+Si) abundance ratio of planet building blocks estimated from the host star chemistry versus Fe/(Mg+Si) ratio from the planets as estimated by mass and radius and using a detailed interior model (18). The estimates for planets are based on the assumption that all iron resides in the core only (left panel) or iron is assumed to be present in both mantle and core (right panel). The symbols are color-coded by the equilibrium temperature of the planets. The black dashed lines represent the results of the OLS linear regression for super-Earths. The error bars of Fe/(Mg+Si) star show one standard deviation. The error bars of  $f_{iron,planet}$  cover the interval between the 16th and the 84th percentiles.